K. Wang and C. T.-C. Nguyen, "High-order micromechanical electronic filters," *Proceedings*, 1997 IEEE International Micro Electro Mechanical Systems Workshop, Nagoya, Japan, Jan. 26-30, 1997, pp. 25-30.

High-Order Micromechanical Electronic Filters

Kun Wang and Clark T.-C. Nguyen

Center for Integrated Sensors and Circuits
Department of Electrical Engineering and Computer Science
University of Michigan
Ann Arbor, Michigan 48109-2122

ABSTRACT

Third-order, micromechanical bandpass filters comprised of three folded-beam resonators coupled by flexural mode springs are demonstrated using an IC-compatible, polysilicon surface-micromachining technology. The use of quarter-wavelength coupling beams attached to resonators at their folding-trusses is shown to suppress passband distortion due to finite-mass nonidealities, which become increasingly important on this micro-scale. A balanced, 300 kHz, prototype, three-resonator micromechanical filter is demonstrated with filter Q=590 and stopband rejection greater than 38 dB.

I. INTRODUCTION

Vibrating mechanical tank components, such as crystal and SAW resonators, are widely used to implement bandpass filters in the RF and IF stages of heterodyning transceivers. Due to orders of magnitude higher quality factor Q, filters utilizing such technologies greatly outperform comparable filters implemented using transistor technologies, in insertion loss, percent bandwidth, and achievable rejection [1]. However, being off-chip components, these mechanical devices must interface with integrated electronics at the board level, and this constitutes an important bottleneck to miniaturization and performance of heterodyning transceivers.

The rapid growth of micromachining technologies, which yield high-Q on-chip mechanical resonators [2] may now make miniaturized, single-chip heterodyning transceivers possible. With Q's of over 80,000 [3] under vacuum and center frequency temperature coefficients in the range of -10 ppm/^{o}C (several times less with nulling techniques) [4], polycrystalline silicon micromechanical resonators (abbreviated "μresonators") can serve well as miniaturized substitutes for crystals in a variety of high-Q oscillator and filtering applications [3,9]. To date, two-resonator (i.e., second-order) prototypes of such filters have been demonstrated from LF (e.g., 20 kHz [5]) to HF (e.g., 8.5 MHz [6]). For use in communications, however, sharper roll-offs and larger stopband rejections are required, and thus, much higher order must be achieved. For the majority of mechanical bandpass filter designs, the order is synonymous with the number of resonators used. However, due to increased susceptibility to passband distorting mismatches and parasitics, micro-scale mechanical filters utilizing three or more resonators have not yet been achieved. The present work extends the order of μmechanical filters to third, reporting on the design, fabrication, and performance of a prototype, planar IC-processed, three-resonator micromechanical bandpass filter centered at 300 kHz with a bandwidth of 510 Hz, stopband rejection exceeding 38 dB, and 20dB-down shape factor as small as 1.45.

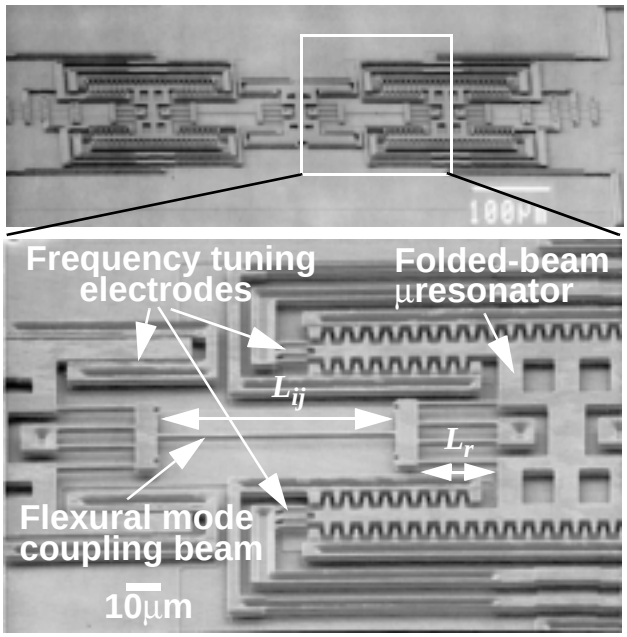

Fig. 1: Wide-angle and close-in SEMs of a prototype, 300 kHz, three-resonator, micromechanical filter.

II. FILTER STRUCTURE AND OPERATION

Figure 1 presents scanning electron micrographs (SEMs) of the prototype, 300 kHz, third-order micromechanical filter, indicating various components and dimensions. An overhead-view schematic of this filter is presented in Fig. 2(a), which provides additional details and associated pickoff electronics.

As shown, this mechanical filter is comprised of three folded-beam μmechanical resonators [2] mechanically coupled at their folding-trusses by soft, flexural-mode springs. The end resonators, which provide the filter inputs and outputs, feature capacitive-comb-transducers for enhanced linearity. In addition, these resonators, as well as the center resonator, are equipped with parallel-plate-capacitive transducers capable of tuning their frequencies. The entire μmechanical filter structure, including resonators and coupling springs, is constructed of doped (conductive) polycrystalline silicon, and is suspended 2 μm over a uniform, doped-polysilicon ground plane that underlies the suspended structure at all points. This ground plane is required to prevent electrostatic pull-in of the structure into substrate, which can occur for structure-to-substrate voltage differences greater than 68 V.

The spring-coupled, three-resonator system of Fig. 2(a) exhibits three mechanical resonance modes with closely spaced frequencies that define the filter passband. The center frequency of the filter is determined primarily by the frequencies of the constituent resonators, while the spacings

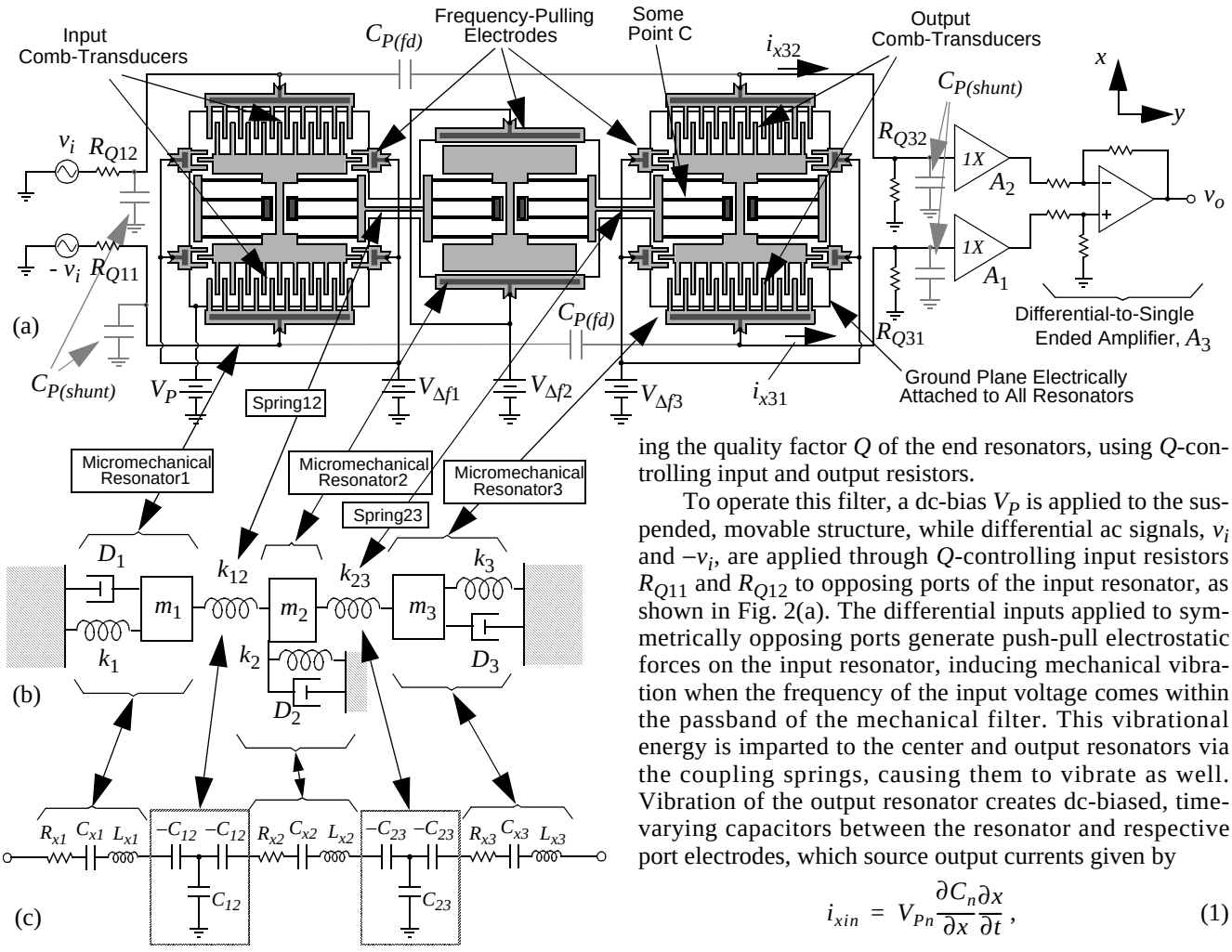

Fig. 2: (a) Overhead schematic of the prototype micromechanical filter with operation electronics. (b) Equivalent lumped parameter mechanical circuit. (c) Equivalent LCR network.

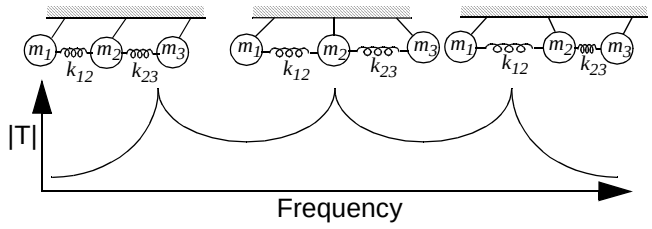

Fig. 3: Mode shapes of the micromechanical filter and their corresponding frequency peaks.

between modes (i.e., the bandwidth) is determined by the stiffnesses of the coupling springs. As shown in Fig. 3, each mode corresponds to a distinct, physical mode shape: in the lowest frequency mode, all resonators vibrate in phase; in the middle frequency mode, the center resonator ideally remains motionless, while the end resonators vibrate 180° out of phase; and finally, in the highest frequency mode, each resonator is phase-shifted 180° from its adjacent neighbor. Without additional electronics, the complete mechanical filter exhibits the jagged passband seen in Fig. 3. As will be shown in Section III, the passband can be flattened by lowering the quality factor Q of the end resonators, using Q-controlling input and output resistors.

To operate this filter, a dc-bias V_P is applied to the suspended, movable structure, while differential ac signals, v_i and $-v_i$, are applied through Q-controlling input resistors R_{Q11} and R_{Q12} to opposing ports of the input resonator, as shown in Fig. 2(a). The differential inputs applied to symmetrically opposing ports generate push-pull electrostatic forces on the input resonator, inducing mechanical vibration when the frequency of the input voltage comes within the passband of the mechanical filter. This vibrational energy is imparted to the center and output resonators via the coupling springs, causing them to vibrate as well. Vibration of the output resonator creates dc-biased, time-varying capacitors between the resonator and respective port electrodes, which source output currents given by

$$i_{xin} = V_{Pn}\frac{\partial C_n}{\partial x}\frac{\partial x}{\partial t}, \qquad (1)$$

where x is displacement (defined in Fig. 2(a)), C_n is the resonator-to-electrode capacitance at port n of resonator i, and V_{Pn} is the dc-bias voltage applied across C_n.

As shown in Fig. 2(a), the differential output currents i_{x31} and i_{x32} are directed through output Q-controlling resistors R_{Q31} and R_{Q32} forming voltages across these resistors which are sensed by buffers A_1 and A_2, then directed to the differential-to-single-ended converter A_3.

III. FILTER DESIGN

Figure 4 presents an ideal bandpass filter spectrum and defines parameters typically used for filter specification. Design techniques that yield such filter responses using LC ladders are quite mature, and large databases governing LC ladder filter design are readily available [7].

For this reason, and for ease of simulation, the micromechanical filter of Fig. 2(a) is realized by first designing an LC ladder version to fit the desired specification. The elements in the LC ladder design are then matched to lumped mechanical equivalents via electromechanical analogy, where inductance, capacitance, and resistance in the electrical domain equate to mass, compliance, and damping, respectively, in the mechanical domain. Figure 2(b) explicitly depicts the equivalence between the actual mechanical filter and a lumped mass-spring-damper system, which in turn, equates to an LC ladder network (Fig. 2(c)) corresponding to the required bandpass filter specification. As shown, for this particular electromechani-

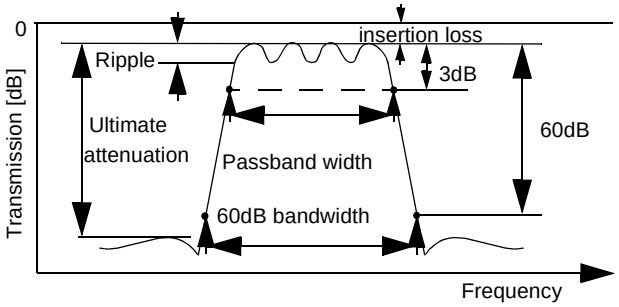

Fig. 4: Parameters typically used for filter specification.

cal analogy (the current analogy), each constituent resonator corresponds to a series LCR tank, while each coupling spring ideally corresponds to a T-network of capacitors, with the whole coupled network corresponding to an LC ladder bandpass filter.

To minimize susceptibility to planar IC fabrication tolerances, the resonators comprising a μmechanical filter should have identical resonance frequency and should otherwise be identical in so much as possible (i.e., identical spring stiffnesses and effective masses). In addition, symmetrical coupled resonator filter designs that utilize symmetrically identical coupling springs on each half of the filter are most appropriate. These design strategies take specific advantage of the good matching tolerances achievable via planar IC fabrication.

Coupled Resonator Filter Design.

Various filter types can be implemented via LC ladder polynomial synthesis techniques, including Chebyshev, linear phase, elliptic, and maximally flat Butterworth. Although filters can be designed via direct synthesis from describing polynomials, this procedure is often no longer required, since all-pole filter designs are widely tabulated in so called filter cookbooks [7]. For the coupled resonator μmechanical filters of this work, tables of "normalized k and q values" are most convenient [7]. Here, the k's correspond to normalized coupling factors, while the q's correspond to normalized values of end resonator quality factor. To de-normalize these tabulated values for a specific filter with center frequency f_o and bandwidth BW, the following relations are used

$$K_{ij} = \frac{BW}{f_o} k_{ij} \text{ and } Q_i = \frac{f_o}{BW} q_i , \qquad (2)$$

where k_{ij} and K_{ij} are the normalized and denormalized coupling factors, respectively, between resonators i and j, while q_i and Q_i are the normalized and denormalized quality factors, respectively, required of end-resonator i (i=1,3). Using these values, the required values of capacitance and inductance making up an LC ladder can be determined. Alternatively, for the case of all-pole filters, the coupling spring constants can be directly determined without reference to an LC ladder using

$$k_{sij} = k_r K_{ij} , \qquad (3)$$

where k_r is the spring constant of the adjacent resonators (assumed identical for all resonators).

Thus, from (2) and (3), a μmechanical bandpass filter with center frequency f_o and bandwidth BW can be realized using a structure comprised of identical resonators, each with resonance frequency f_o, coupled by springs with stiffnesses k_{sij}.

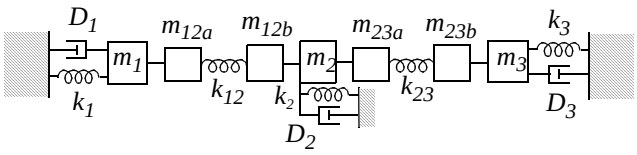

Fig. 5: Equivalent mechanical circuit for the filter of Fig. 2(a) for the case where coupling springs have finite mass.

Micromechanical Resonator Design.

The folded-beam micromechanical resonators used in this design operate at frequencies higher than previously reported and differ from previous versions in that their suspending beams and folding trusses are similar in size. Closed form equations [2] no longer accurately predict their resonance frequencies, so distributed matrix techniques are utilized for analytical design, with verification by finite element simulation.

The effective lumped mass m_r and spring constant k_r of a folded-beam resonator are functions of the location y (see Fig. 2(a)) on the resonator and can be defined by

$$m_r\big|_{y=y_c} = \frac{KE_{tot}}{(1/2)v_c^2} \text{ and } k_r\big|_{y=y_c} = \omega_o^2 m_r\big|_{y=y_c} , \qquad (4)$$

where v_c is the velocity at some point $y = y_c$. KE_{tot} is the total kinetic energy in the spring-mass system given by [8]

$$KE_{tot} = \frac{1}{2}\omega_o^2 X_o^2 M_o , \qquad (5)$$

where

$$M_o = M_p + \frac{1}{4}M_t + \frac{12}{35}M_b \qquad (6)$$

is the effective equivalent mass seen at any point on the resonator shuttle, X_o is the shuttle displacement amplitude, and M_p, M_t, and M_b are the masses of the shuttle plate, folding truss, and the sum of all folded beams, respectively.

With knowledge of the equivalent lumped mass m_r and stiffness k_r of the constituent resonators, the equivalent LCR circuit elements for each resonator are as follows [3]:

$$C_x = \frac{\eta_n^2}{k_r} \qquad R_x = \frac{\sqrt{k_r m_r}}{Q\eta_n^2}$$
$$L_x = \frac{m_r}{\eta_n^2} \qquad \eta_n = V_{Pn}\frac{\partial C_n}{\partial x} , \qquad (7)$$

where Q is quality factor, and $\partial C_n/\partial x$ is the change in resonator-to-electrode capacitance per unit displacement at input port n (n=1,2). To design the mechanical resonators comprising a μmechanical filter, k_r, m_r, and η_n are chosen to match values of C_x and L_x required by the tanks of an appropriate LC ladder, or vice versa.

Coupling Beam Design.

The equivalent mechanical circuit shown in Fig. 2(b) models an ideal case, where the springs coupling the resonators are massless. In reality, the coupling springs have finite mass that, without special design precautions, can add to adjacent resonators, shifting their frequencies and causing distortion of the filter passband. In particular, as shown in Fig. 5, unequal spring mass additions to the center resonator relative to the end resonators cause mismatches in res-

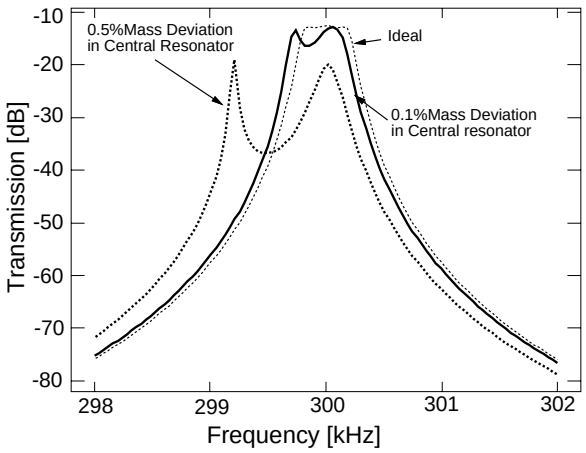

Fig. 6: Simulations demonstrating the effect of increasing center resonator mass (end resonators remaining constant) on the filter passband.

onator frequencies, which then lead to passband distortion. Note that this phenomenon is absent for two-resonator filters, but can have a major impact on higher-order filters, as illustrated by Fig 6, which presents SPICE simulations modelling the effect of increases in center resonator mass over that of the end resonators for a three-resonator filter.

The influence of finite coupling spring mass can be greatly suppressed by design methods that model coupling beams as impedances and that strategically take advantage of the distributed, transmission-line behavior of flexural-mode coupling beams at the filter center frequencies of present interest. Due to this distributed behavior, the amount of mass (and stiffness) added to the adjacent resonators by a given coupling beam is a function of its length, L_{ij}. When L_{ij} corresponds to an effective quarter-wavelength of the filter center frequency, the impedance of the coupling beam as seen by adjacent resonators is effectively massless. Thus, by restricting the coupling beam lengths to effective quarter-wavelengths, center frequency shift and passband distortion of high-order filters is avoided, and the equivalent mechanical and electrical circuits for the μmechanical filter of this work return to those shown in Fig. 2.

The flexural mode coupling beam used in this design corresponds to a quarter-wavelength when its length L_{ij} and width W_{ij} are chosen to simultaneously satisfy the following expressions [8]

$$\cos\alpha\sinh\alpha + \sin\alpha\cosh\alpha = 0 \qquad (8)$$

$$k_{sij} = -\frac{EI\alpha^3(\sin\alpha + \sinh\alpha)}{L_{ij}^3(\cos\alpha\cosh\alpha - 1)}, \qquad (9)$$

where $\alpha = L_{ij}(\rho A\omega_o{}^2/E/I)^{0.25}$, $I = hW_{ij}{}^3/12$, $A = W_{ij}h$, and k_{sij} is given by (3).

The above quarter-wavelength spring design technique is especially important for high-order micro-scale mechanical filters, which have coupling beam masses on the same order as that of the resonators. This becomes an increasing problem as frequencies scale upwards, since resonator mass must continue to shrink to accommodate, while coupling beam mass reduces much more slowly [9].

Low Velocity Coupling.

Rather than attach coupling beams to resonator shuttle masses, as has been done in previous two-resonator work [5], this filter design couples resonators at their folding trusses, which are moving at half the velocity of their shuttle masses. Given that the magnitude of the shuttle mass velocity is $V_o = \omega_o X_o$, (4) yields

$$m_r = \frac{KE_{tot}}{(1/8)(\omega_o^2 X_o^2)} = 4M_o \text{ and } k_r = 4k_o, \qquad (10)$$

where k_o is the effective spring stiffness seen at the shuttle location. Thus, both m_r and k_r are four times larger at the truss than at the shuttle. From (3), this means that the coupling spring stiffness must also be four times larger if coupling occurs at the truss rather than at the shuttle, and this greatly simplifies the coupling spring design problem. Without the increase in k_{sij} provided by this low velocity coupling strategy, deep submicron coupling beam widths would be required for reasonable L_{ij}'s.

Filter Termination.

As mentioned in Section II, without the termination resistors R_{Qin} shown in Fig. 2(a), the passband of the μmechanical filter would be as shown in Fig. 3, comprised of three peaks, with excessive ripple. To obtain the designed value of passband ripple, the Q of the end resonators must be controlled to equal the calculated values of Eq. (2). For the design of Fig. 2(a), this is most easily done by placing resistors R_{Q1n} in series with each input and resistors R_{Q2n} in shunt with each output. The required resistor values are given by

$$R_{Qin} = \frac{1}{2}\left(\frac{Q_{init}}{Q_i} - 1\right)R_x, \; i = 1, 3 \qquad (11)$$

where R_x is defined in (7), Q_{init} is the initial, uncontrolled quality factor of the constituent resonators, Q_i is defined in (2), and n refers to a particular port of end resonator i.

The value of R_{Qin} greatly influences the magnitude of input-referred noise of the filter, as well as the degree of parasitic-induced passband distortion. To minimize these effects, R_{Qin} must be minimized. From (11), this is best accomplished by minimizing the value of R_x, which, with reference to (7), is in turn best accomplished by maximizing $\partial C_n/\partial x$, assuming that V_P is restricted by power supply limitations. $\partial C_n/\partial x$ is best maximized by minimizing the gap spacing between resonator and electrode comb fingers. Alternatively, if more transducer ports are available, active Q-control is also possible, which eliminates series resistors and offers both noise and dynamic range advantages [9].

IV. PRACTICAL DESIGN ISSUES

In addition to the above theoretical issues, practical design issues, such as resiliency against fabrication mismatch and against parasitic elements, must also be considered. Figure 6 from Section IV showed that even slight mismatches between constituent resonators can lead to significant passband distortion. In addition, as shown in Fig. 7, parasitic capacitance shunting and connecting the filter inputs and outputs can also greatly distort the passband. In particular, shunt capacitance can interact with Q-controlling resistors to cause excessive phase lag, which then distorts the passband and can preclude termination-based passband-flattening.

To correct for fabrication mismatch tolerances, each resonator comprising the filter is equipped with parallel-plate-capacitor transducers, which due to their nonlinearity,

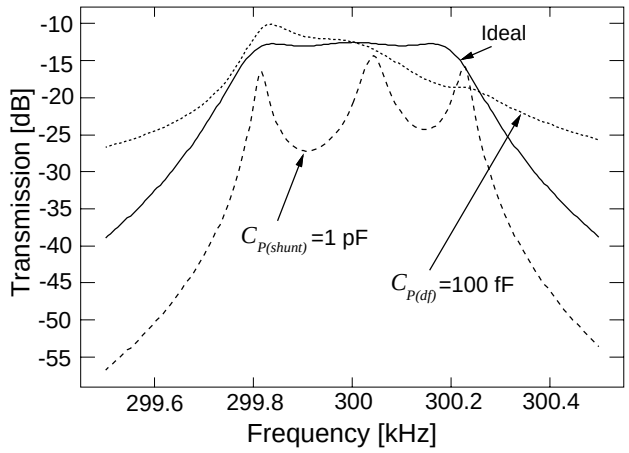

Fig. 7: SPICE simulations illustrating the effect of shunt and feedthrough parasitic capacitance on the filter passband. See Fig. 2(a) for parasitic capacitor definitions.

allow frequency tuning of resonators via inherent V_P-dependent electrostatic spring constants [10]. The dependence of frequency on tuning voltage $V_{\Delta fi}$ for resonator i is a function of the tuning electrode-to-resonator overlap capacitance C_{oi}, and is given by

$$f_{oi}' = f_o\left(1 - \frac{(V_P - V_{\Delta fi})^2 C_{oi}}{k_r d_i^2}\right)^{1/2}, \qquad (12)$$

where d_i is the capacitor gap spacing.

To minimize the effects of parasitic feedthrough capacitance, the differential drive and sense scheme depicted in Fig. 2(a) is utilized. Input and output shunt capacitance is minimized by careful board layout of off-chip electronics.

V. EXPERIMENTAL RESULTS

Several prototype, 300 kHz, high-order, micromechanical bandpass filters were designed using the methods detailed in Sections III and IV, and fabricated using a polysilicon surface-micromachining technology. Table I summarizes design data for one of the filters, with reference to the parameters and dimensions indicated in Figs. 2 and 4.

A custom-built vacuum chamber, with pc board support and feedthroughs allowing electrical connections to external instrumentation, was utilized to characterize both μmechanical resonators and filters. Devices under test were bonded to carefully grounded metal packages and interfaced with off-chip electronics at the board-level, taking special precautions to minimize shunt capacitance at the filter input and output nodes and to null out feedthrough capacitance so much as possible. A roughing pump was utilized to evacuate the chamber to pressures on the order of 40 mTorr before testing devices.

Stand-alone, 300 kHz folded-beam, comb-driven μmechanical resonators were tested first, using the described vacuum chamber along with op-amp based transresistance amplifiers and an HP 4195A Network/Spectrum Analyzer. From measured transconductance spectra, the resonators were found to have *Q's* greater than 25,000. The average resonance frequency mismatch for four resonators in close proximity was found to be 0.7%, which is consistent with previously measured values [3]. This degree of frequency mismatch is sufficient to cause significant passband distortion and must be corrected using trimming or tuning strategies to obtain a given filter specification.

Table I: Three-Resonator μMechanical Filter Data

Parameter	Value	Units
μRes. Folded-Beam Length, L_r	32.8	μm
μRes. Folded-Beam Width, W_r	2	μm
Structural Layer Thickness, h	2	μm
μResonator Effective Mass, m_r	$1.52\text{x}10^{-10}$	kg
μResonator Spring Constant, k_r	135.4	N/m
Comb-Finger Gap Spacing, d	1	μm
Comb-Finger Overlap, L_o	5	μm
Electromechanical Coupling, η	$1.48\text{x}10^{-7}$	VF/m
Coupling Beam Length, L_{12}=L_{23}	75.2	μm
Coupling Beam Width, W_{12}=W_{23}	0.8	μm
Filter Center Frequency, f_o (=$\omega_o/2\pi$)	299.42	kHz
Filter Bandwidth, BW	510	Hz
Filter Q	590	—
Filter Stopband Rejection	38	dB
Filter Shape Factor, BW_{-20dB}/BW_{-3dB}	1.45	—
Filter Insertion Loss	<3	dB
Young's Modulus, E	150	GPa
Density of Polysilicon, ρ	2300	kg/m^3
Filter DC-Bias, V_P	150	V
μRes1 Freq. Tuning Voltage, $V_{\Delta f1}$	77.6	V
μRes2 Freq. Tuning Voltage, $V_{\Delta f2}$	0	V
μRes3 Freq. Tuning Voltage, $V_{\Delta f3}$	77.6	V
Q-Control Resistors, R_{Q1n}=R_{Q2n}	470	kΩ

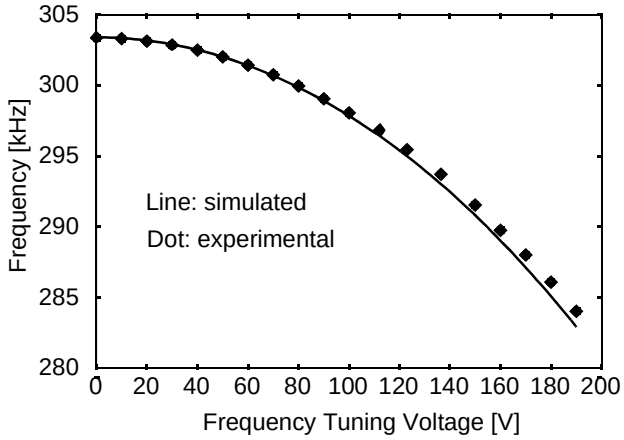

Fig. 8: Measured plot of resonance frequency versus tuning voltage for a stand-alone end-resonator.

To demonstrate the frequency tuning range provided by the parallel-plate capacitor tuning structures described in Section IV, Fig. 8 presents a plot of resonance frequency versus tuning voltage $V_{\Delta f}$ for a stand-alone end-resonator, measured using the described set-up. Here, a tuning range of over 2% is demonstrated for a 50 V range in $V_{\Delta f}$— quite adequate for compensation of measured mismatches.

Micromechanical filters were then characterized, again using the custom-built vacuum chamber, with board-level electronics hooked up as in Fig. 2(a). First, two-resonator

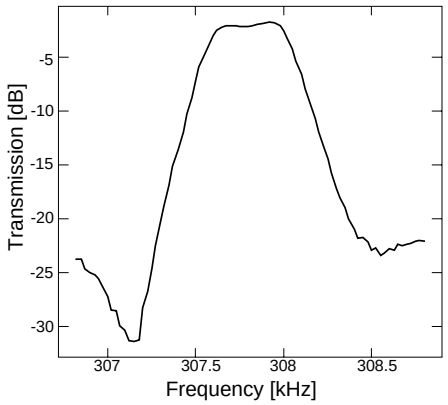

Fig. 9: Transmission spectrum for a 307.8 kHz two-resonator micromechanical filter.

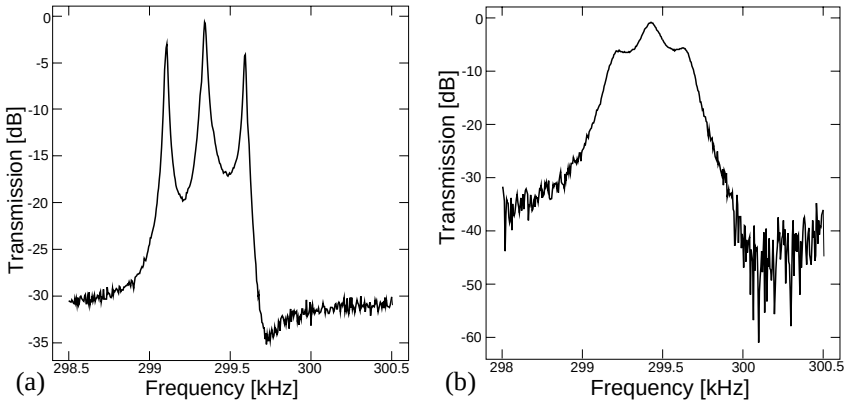

Fig. 10: Measured transmission spectra for the prototype, three-resonator micromechanical filter (a) after frequency tuning to achieved matched resonators; and (b) after passband correction using *Q*-controlling resistors.

filters were tested for later comparison with higher-order versions. Figure 9 presents the transmission spectrum for a two-resonator filter, showing a stopband rejection of 21 dB. Characterization of three-resonator filters was then accomplished using the following procedure:

(1) tune resonance frequencies via $V_{\Delta f}$ to achieve symmetrical modal frequencies; then

(2) insert proper values of R_{Qin} to flatten the filter passband to the specified ripple.

The measured transmission spectra after each step of this procedure are presented in Fig. 10.

The measured spectrum of Fig. 10(b) achieves many of the design specifications, including a bandwidth of 510 Hz, a 20dB-down shape factor of 1.45, insertion loss less than 3 dB, and a stopband rejection greater than 38 dB—this is 17 dB better than obtained via the two-resonator filter of Fig. 9. However, it still displays more passband ripple than desired. As can be seen through comparison with Fig. 7, this is caused by board-level parasitic capacitance shunting the filter input and output ports, and interacting with termination resistors R_{Qin} to cause excessive phase lag. Several strategies are available to alleviate this passband distortion, including (1) reducing the R_{Qin}'s by decreasing the resonator-to-electrode comb-finger gap spacings; and (2) reducing shunt capacitance by more careful board-layout or by fully integrating the entire filter, along with sense and *Q*-controlling electronics, onto a single chip. The first of these also allows more reasonable (smaller) values of dc-bias voltage V_P [6]. These options are both consistent with current trends in planar IC and MEMS technologies, both of which are moving towards higher-aspect ratios and increased integration.

VI. CONCLUSIONS

High-*Q*, third-order, bandpass, micromechanical filters have been designed and demonstrated in an IC-compatible polysilicon surface-micromachining technology. For design of these filters, electromechanical analogies proved very useful and allowed the use of well-established LC ladder filter design tables as starting points. Passband distortion due to the finite mass of coupling springs was shown to have significant impact on high-order filters, especially on the micro-scale, where resonators and couplers can have comparable masses. Parasitic elements were also shown to more heavily influence the passband of high-order filters. Quarter-wavelength coupling beams, low velocity coupling, fully-balanced operation, frequency-tunable resonators, and maximum electromechanical coupling can all greatly alleviate these nonideal effects and are key to successful micro-scale mechanical filter implementation. These design strategies will likely become increasingly important as the frequency and order of micromechanical filters rise to accommodate today's cellular needs, and beyond.

Acknowledgments: The authors are grateful for fabrication support from the staff of the University of Michigan's Microelectronics Fabrication Laboratory, particularly from Qing Bai and Frank Bannon III. This work was supported by a grant from the National Science Foundation.

References:

[1] H. Khorramabadi and P. R. Gray, "High-frequency CMOS continuous-time filters," *IEEE J. Solid-State Circuits*, vol. SC-19, No. 6, pp. 939-948, Dec. 1984.

[2] W. C. Tang, T.-C. H. Nguyen, and R. T. Howe, "Laterally driven polysilicon resonant microstructures," *Sensors and Actuators*, **20**, 25-32, 1989.

[3] C. T.-C. Nguyen, "Micromechanical resonators for oscillators and filters," *Proceedings*, 1995 IEEE International Ultrasonics Symposium, Seattle, WA, pp. 489-499, Nov. 7-10, 1995.

[4] C. T.-C. Nguyen and R. T. Howe, "Microresonator frequency control and stabilization using an integrated micro oven," *Digest of Technical Papers*, the 7th International Conference on Solid-State Sensors and Actuators (Transducers'93), Yokohama, Japan, pp. 1040-1043, June 7-10, 1993.

[5] L. Lin, C. T.-C. Nguyen, R. T. Howe, and A. P. Pisano, "Micro electromechanical filters for signal processing," *Technical Digest*, IEEE Micro Electromechanical Systems Workshop, Travemunde, Germany, pp. 226-231, Feb. 4-7, 1992.

[6] F. D. Bannon III, J. R. Clark, and C. T.-C. Nguyen, "High frequency microelectromechanical IF filters," *Technical Digest*, IEEE International Electron Devices Meeting, San Francisco, California, December 8-11, 1996, pp. 773-776.

[7] A. I. Zverev, *Handbook of Filter Synthesis*. New York: John Wiley & Sons, 1967.

[8] R. A. Johnson, *Mechanical Filters in Electronics*, New York: John Wiley & Sons, 1983.

[9] C. T.-C. Nguyen, "High-*Q* micromechanical oscillators and filters for communications," to be published in the *Proceedings* of the 1997 IEEE International Symposium on Circuits and Systems, Hong Kong, June 9-12, 1997.

[10] R. T. Howe and R. S. Muller, "Resonant microbridge vapor sensor," *IEEE Trans. Electron Device*s, ED-33, pp. 499-506, 1986.